Title
RAPID SOLIDIFICATION MICROSTRUCTURES IN AUSTENITIC Fe-Ni ALLOYS

Authors
Hayzelden, C.
Rayment, J.J.
Cantor, B.

Publication Date
1982-08-01

LBL-14812
Preprint

Lawrence Berkeley Laboratory
UNIVERSITY OF CALIFORNIA

Materials & Molecular
Research Division

Submitted to Acta Metallurgica

RAPID SOLIDIFICATION MICROSTRUCTURES IN AUSTENITIC Fe-Ni ALLOYS

C. Hayzelden, J.J. Rayment and B. Cantor

August 1982

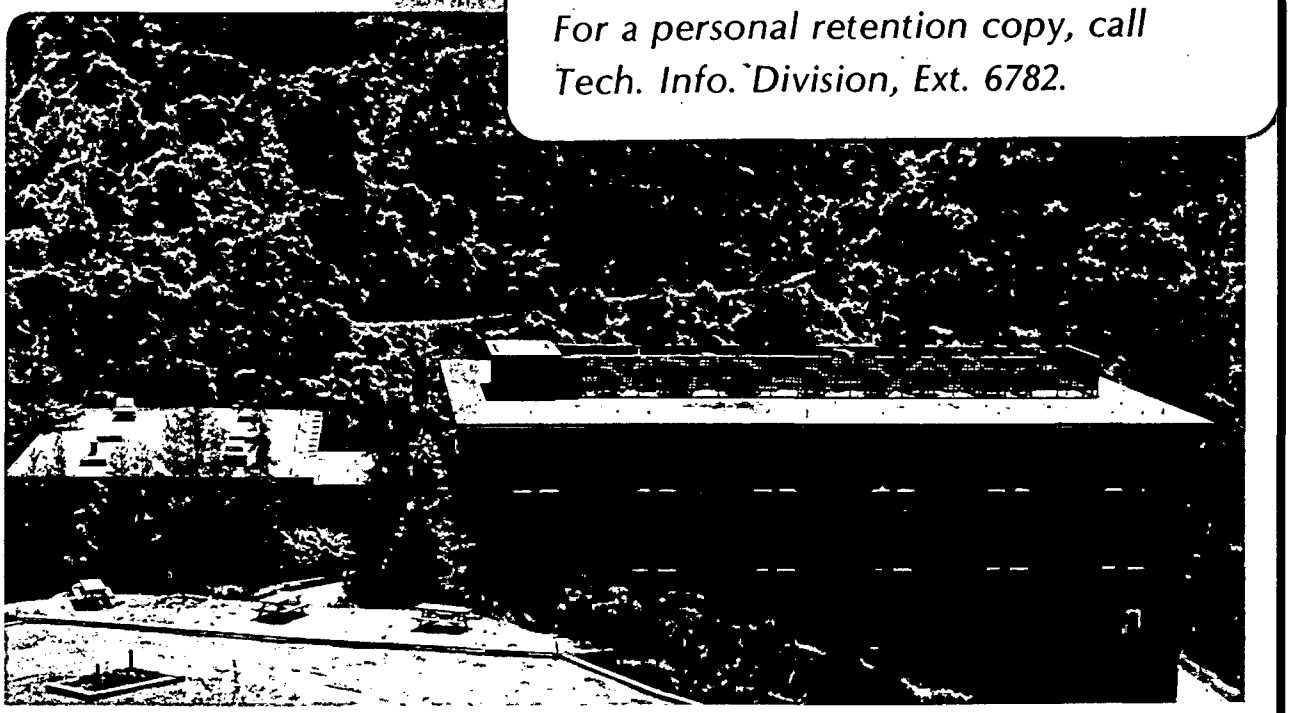

Prepared for the U.S. Department of Energy under Contract DE-AC03-76SF00098

DISCLAIMER

RAPID SOLIDIFICATION MICROSTRUCTURES IN AUSTENITIC Fe-Ni ALLOYS

C. Hayzelden[+], J. J. Rayment[*] and B. Cantor[+]

School of Engineering & Applied Sciences
University of Sussex, Brighton, Sussex, UK

ABSTRACT

The microstructures of rapidly solidified austenitic Fe-Ni alloys have been investigated by a combination of scanning and transmission electron microscopy, X-ray diffraction and X-ray microanalysis. Temperature measurements during rapid solidification have been used to interpret the results. Rapid solidification is shown to be a non-Newtonian cooling process, with high liquid undercooling before the onset of solidification, followed by adiabatic recalescence while solidification takes place. Detailed composition measurements provide direct evidence that high liquid undercooling causes massive segregation-free solidification, but recalescence can produce a breakdown in the later stages of solidification to a cellular, segregated solidification structure.

INTRODUCTION

In recent years, there has been considerable scientific and technological interest in using rapid solidification processing, with cooling rates during solidification of $> 10^5$ K s^{-1}, to produce new microstructures and

---

[+]Present Address: Department of Metallurgy and Science of Materials, University of Oxford, Oxford, UK

[*]Present Address: Materials and Molecular Research Division, Lawrence Berkeley Laboratory, University of California, Berkeley, CA, USA

improved properties in a variety of metallic alloys (1-4). Although much emphasis has been placed in the literature upon the study of glassy metals, it is only lately that rapid solidification of crystalline metals has begun to be investigated in similar detail. In general, it has proved quite difficult to predict or interpret the microstructures of rapidly solidified crystalline alloys. There are several reasons for this: (a) the difficulty of measuring cooling rates during rapid solidification (5,6); (b) the inherent variability of many rapid solidification processes (5); (c) the difficulty of resolving fine-scale rapidly solidified microstructures (7,8) and (d) the complex alloy systems which often have been studied, such as high-speed tool steels (9) and nickel-base superalloys (7).

The objective of the present work was to investigate microstructures and segregation patterns in a simple binary alloy system after rapid solidification under conditions of known cooling rate. The alloys which were studied were austenitic Fe-Ni, and two rapid solidification techniques were used, two-piston quenching (TPQ) and melt-spinning (MS). Cooling rates during two-piston quenching were measured with a rapid response thermocouple embedded in one of the pistons, and cooling rates during melt-spinning were measured by calibrated colour photography. Austenitic Fe-Ni solidification microstructures were characterised by a combination of X-ray diffraction, microhardness testing, scanning electron microscopy (SEM), conventional and scanning transmission electron microscopy (TEM and STEM), and wavelength and energy dispersive X-ray spectroscopic analysis (WDS and EDS).

EXPERIMENTAL TECHNIQUE

Ingots of Fe-25, 30, 35 and 40%Ni were prepared by induction-melting

99.99% pure Fe and Ni in recrystallised alumina crucibles under a dynamic argon atmosphere. Two-piston quenched Fe-25%Ni specimens were obtained under an argon atmosphere by levitation-melting individual samples of between 0.5-0.8g, followed by quenching between two magnetically-accelerated, polished copper pistons with a closing velocity of $13ms^{-1}$. The details of this TPQ technique have been described elsewhere (5,10). The resulting TPQ specimens were thin discs, typically 20-30mm in diameter and 60-100μm thick. MS Fe-30, 35 and 40%Ni specimens were obtained under a helium atmosphere by induction-melting individual samples of between 5-10g in quartz nozzles with an orifice diameter of 1mm, followed by ejection with a helium overpressure of 8psi onto the surface of a polished copper drum, rotating with a surface speed of $28\ ms^{-1}$. The resulting MS specimens were thin ribbons, typically 1.5-2.0m long, 2-3mm wide, and 40-80μm thick.

The TPQ cooling rates have been measured previously (5,11) during rapid solidification of TPQ pure Fe specimens, using an oscilloscope to monitor the output of a rapid-response thermocouple embedded in one of the copper pistons. Full details of this precedure have been described elsewhere (5,12). MS cooling rates were measured from colour photographs during rapid solidification of MS pure Fe and Fe-26%Ni-2%Mn ribbons. Colour-temperature calibration was obtained as follows. The Fe ribbon was subsequently resistance-heated in the same helium atmosphere used for melt-spinning, the ribbon temperature was monitored with a pyrometer, and the ribbon was rephotographed at different temperatures with the same film used during melt-spinning. This colour-temperature calibration was used to convert the colour variation along the ribbon during

melt-spinning into a temperature distribution, and cooling rates were then calculated from the ribbon velocity of $28ms^{-1}$.

The phases present in TPQ and MS specimens were determined by X-ray diffraction using Mo K_α radiation on either a Siemens diffractometer or a Huber-Guinier camera. Both TPQ and MS specimens were polished to 1μm diamond and etched in 2% nital for (a) SEM microstructural examination and WDS bulk composition analysis on a JEOL JSM35C microscope fitted with a vertical X-ray spectrometer, and (b) Vickers microhardness testing on a Leitz optical microscope using low loads to prevent stress relaxation near specimen edges. Other TPQ and MS specimens were jet-electropolished in 20% perchloric acid/80% methanol for TEM and STEM microstructural examination and EDS segregation analysis on a JEOL 120C microscope fitted with a Link Systems 860 x-ray detector and analyser.

For WDS bulk composition measurements, compositions were calculated from:

$$C_{Fe} = k_1 N_{Fe}/N^{\circ}_{Fe} \qquad (1)$$

$$C_{Ni} = k_2 N_{Ni}/N^{\circ}_{Ni} \qquad (2)$$

where C_{Fe} and C_{Ni} are specimen weight fractions of Fe and Ni, N_{Fe} and N_{Ni} are number of X-ray counts in Fe and Ni K peaks in a specimen X-ray spectrum after computer-fitting to subtract background counts and to allow for peak overlap, and N°_{Fe} and N°_{Ni} are equivalent counts from pure Fe and Ni standards obtained under identical conditions. Values of k_1 and k_2 were calculated iteratively using standard methods for atomic number, absorption and fluorescence corrections.

Energy Dispersive Spectroscopic analysis was used for high-resolution measurements of fine-scale composition variations within a given TEM

specimen. These measurements were quite difficult. The X-ray detector was in the specimen plane of the TEM, so with zero specimen tilt or a thin specimen, the X-ray count rate was too low for good counting statistics. On the other hand, with a high tilt angle or thick specimen, the region of X-ray generation became too large for good resolution. For low experimental scatter and acceptable resolution, specimen thicknesses were between 100-300nm, tilt angles were between 20-30°, and the resolution was ∿50nm. Compositions were calculated from:

$$C_{Fe} + C_{Ni} = 1 \qquad (3)$$

$$C_{Fe}/C_{Ni} = k_3 N_{Fe}/N_{Ni} \qquad (4)$$

where equation (3) assumes an impurity-free specimen, and the value of k_3 was computed iteratively allowing for detector efficiency, atomic number and absorption corrections. Unlike the WDS analysis, the EDS analysis correction procedure was not suitable for absolute composition measurements, because of the difficulty of estimating specimen thickness for the absorption correction. However, this source of error in calculating k_3 was insignificant for measuring relative variations in composition over small regions of a given TEM specimen.

RESULTS

Table 1 shows the results of the cooling rate measurements. Under the conditions used to prepare austenitic TPQ Fe-25%Ni, the cooling rate was in the range $4 \times 10^6 - 10^7$ K s^{-1} at 1500°C (near the melting point), falling to $7 \times 10^5 - 2 \times 10^6$ K s^{-1} at 1000°C. Under the conditions used to prepare MS Fe-30, 35 and 40% Ni, the ribbons lost contact with the

copper drum at a temperature of ∿1100°C. While in contact with the drum, between 1600 - 1100°C, the mean cooling rate was 5×10^5 K s^{-1}, approximately one order of magnitude lower than the TPQ technique. After leaving the drum, between 1100 - 900°C, the cooling rate dropped sharply to 10^4 K s^{-1}, approximately two orders of magnitude lower than the TPQ technique.

Chemical compositions of rapidly-solidified TPQ and MS specimens were measured by WDS analysis on the SEM, and the results are given in Table 2. X-ray diffraction showed that all TPQ Fe-25%Ni and MS Fe-30, 35 and 40% Ni specimens were fully austenitic at room temperature, and this was further confirmed by electron diffraction in the TEM. Microhardness results are also included in Table 2. In agreement with previous work (8), TPQ austenitic Fe-25%Ni had a microhardness of ∿270Kg mm^{-2}, and MS Fe-30, 35 and 40% Ni had lower microhardnesses of 150-175 Kg mm^{-2}.

Figures 1 and 2 show typical TEM micrographs from TPQ Fe-25%Ni specimens. In some regions, as shown in Figure 1, the microstructure consisted of fine-scale equiaxed austenite grains. In other regions, as shown in Figure 2, the austenitic grains had convoluted grain boundaries, and appeared to contain low-angle dislocation sub-boundaries. Although equiaxed austenite grains were seen in several areas of different specimens, the majority of electron transparent areas which were examined contained irregular austenite grains as in Figure 2.

Figures 3 and 4 show typical TEM micrographs from MS Fe-Ni ribbons. In order to investigate the early stages of solidification near the surface of the copper drum, some of the TEM specimens were prepared by

jet-electropolishing after the top surface of the ribbon had been removed by grinding. The resulting microstructure consisted of fine-scale equiaxed austenite grains as shown in Figure 3, very similar to the equiaxed austenite grains in Figure 1 found in TPQ specimens. In order to investigate the later stages of solidification, some of the TEM specimens were prepared by jet-electropolishing after the bottom surface of the ribbon had been removed by grinding. The resulting microstructure again consisted of fine-scale equiaxed austenite grains, but the austenite grains contained an internal cellular structure as shown in Figure 4. Selected area diffraction, confirmed that adjacent cells formed part of a single austenite grain. When TEM specimens were prepared without any prior removal of the ribbon by grinding, the microstructure was variable, sometime consisting of cellular austenite grains as in Figure 4, and sometimes consisting of non-cellular austenite grains as in Figure 3.

In general, the austenitic Fe-Ni specimens were difficult to etch for the SEM. However, Figure 5 shows a typical SEM micrograph from a through thickness cross-section of an MS Fe-Ni ribbon. The austenite grains and internal cells were both columnar and, as expected from the TEM micrographs, internal cells were only present near the top surface of the ribbon. The onset of the cellular structure varied in the position between 1/4 - 1/2 way through the thickness of the ribbon. Internal cells were not seen in TPQ Fe-25%Ni specimens.

The diameters of columnar austenite grains and internal cells were measured by a line intercept method, using TEM and SEM micrographs such as Figures 1-5. Table 3 shows the range of results obtained from a large number of measurements from different rapidly solidified specimens. In

TPQ specimens and near the bottom surface of MS ribbons, the austenite grains were $\sim 2\mu m$ in diameter. Near the top surface of the MS ribbons, the austenite grain size increased slightly, with internal cells $\sim 1\mu m$ in diameter. Dislocation density measurements are also shown in Table 3. In TPQ specimens, the dislocation density was $\sim 10^{15}$ lines m^{-2}, whereas in MS ribbons the dislocation density was lower, $\sim 10^{12}$ lines m^{-2}, in agreement with the different microhardness values in Table 2. When the austenite grains contained internal cells, there was a tendency for the dislocations to decorate the cell boundaries. This is shown in Figure 6, where the same region as in Figure 4 has been imaged at a slightly different tilt angle.

Orientations of adjacent austenite grains were investigated by analysing Kikuchi-line patterns obtained by selected area diffraction in the TEM. Figures 8 and 9 show typical sets of results for TPQ and MS specimens. The stereographic projections in Figures 7(b) and 8(b) show the relative orientations of unit stereographic triangles from each of the austenite grains marked in Figures 7(a) and 8(a) respectively. This investigation was repeated in many specimens, and in general the austenite grains had fairly random orientations, and were usually separated by high-angle grain boundaries. As can be seen in Figure 8 however, there was sometimes evidence for a slight <100> texture through the thickness of both the TPQ discs and MS ribbons. In addition, low-angle grain boundaries were occasionally detected, as shown for instance by the similar orientations of grains 3, 7 and 8 in Figure 7 and grains 2 and 4 in Figure 8.

Table 4 shows composition measurements obtained by EDS and analysis from a series of cellular austenitic regions near the top of different

MS Fe-Ni specimens. Many point compositions were measured in each region, and Table 4 quotes in each case the mean cell boundary and mean cell centre compositions, together with their respective standard deviations. The data in Table 4 appear to disagree with the WDS analyses in Table 2, but as mentioned above, no attempt was made to calibrate the EDS analysis method for absolute composition measurements. The significant feature of Table 4 is that in all specimens the Ni concentration at cell boundaries was greater than at cell centres, although the composition difference was small, <1%, almost lost within the experimental scatter. While, therefore not entirely conclusive, the results do indicate that the cellular microstructure in MS austenite grains is associated with Ni segregation into the cell boundaries. Similar experiments on TPQ specimens and on non-cellular regions of MS ribbons showed no evidence of consistent variations in Ni concentration, and individual point measurements of composition were always scattered randomly in a given specimen, within a standard deviation of 0.5-1.0%.

DISCUSSION

Consider a thin parallel-sided specimen, cooling with one face in contact with a cold substrate. The type of cooling experienced by the specimen is determined by the relative magnitude of k, the specimen thermal conductivity, k', the substrate thermal conductivity, and the product hd, where h is the heat transfer coefficient at the specimen/substrate interface, and d is the specimen thickness. When hd is much smaller than k and k', the specimen undergoes Newtonian cooling, with no thermal gradients in specimen or substrate, and with the temperature drop between specimen and substrate concentrated at the specimen/

substrate interface. The rate of heat removal per unit area of specimen/substrate interface is given by:

$$q = h(T - T_s) = d\rho C\dot{T} \qquad (5)$$

where T and T_s are the instantaneous specimen and substrate temperatures, ρ and C are the specimen density and specific heat, and $\dot{T}$ is the instantaneous specimen cooling rate. For a thick substrate, T_s is constant, so the specimen cooling rate is proportional to its temperature and both fall exponentially with time. For non-Newtonian cooling, thermal gradients in specimen and substrate cannot be ignored, and thermal diffusion equations must be solved in both specimen and substrate in order to calculate the specimen cooling rate. In general, analytical solutions cannot be found. However, the mean specimen cooling rate decreases more rapidly with falling specimen temperature than would be expected from the proportionality in Newtonian cooling indicated by equation (5). The extreme case of non-Newtonian cooling is ideal cooling, when k and k' are much smaller than hd. In ideal cooling, there is no effective resistance to heat flow and no temperature drop at the specimen/substrate interface. Other cases of non-Newtonian cooling are referred to as intermediate cooling. With 2-substrate cooling as in the TPQ technique, the comments above still apply, but d should be taken as half the specimen thickness.

Wood and Honeycombe (12) have suggested that rapid solidification of Fe alloys always takes place under Newtonian conditions of cooling. However, the results in Table 1 are clearly non-Newtonian, since TPQ specimen cooling rates are not proportional to specimen temperature. Numerical solutions to specimen and substrate thermal diffusion equations have been obtained by Ruhl (13) for an Fe specimen on a copper substrate

and are also applicable to an Al specimen on a copper substrate (14). Ruhl's calculations have been used to plot mean specimen cooling rates versus specimen thickness, for comparison with measured cooling rates in rapidly solidified Al (14) and Fe (15) alloys. This plot is shown in Figure 9, together with the results in Table 1 and previous data for Al and Fe alloys (14, 15). In general agreement with the previous results, TPQ and MS Fe-Ni specimens undergo intermediate cooling, with a heat transfer coefficient of 10^5 - 10^6 W m^{-2} K^{-1}.

Conventionally solidified Fe-Ni alloys are only austenitic at room temperature when the Ni content is >30%; with lower Ni content, the as-solidified austenite transforms to martensite or ferrite during cooling to room temperature (8,16). In TPQ Fe-Ni alloys, a combination of high cooling rate and small as-solidified austenite grain size has been shown to depress the transformation temperature, so that austenite is retained to room temperature for Ni contents ≥25%Ni (8,17,18). A less marked effect is found in MS Fe-Ni alloys because of the lower cooling rates at low temperatures, and MS Fe-Ni alloys have been shown to be austenitic at room temperatures with ≥29%Ni (19). The present work shows fully austenitic microstructures in TPQ Fe-25%Ni and MS Fe-30, 35 and 40%Ni, and is therefore consistent with previous results.

Two-piston quenched Fe-25%Ni and MS Fe-30, 35 and 40%Ni consist of columnar austenite grains extending through the thickness of the TPQ discs and MS ribbons. This indicates that nucleation takes place on the surface of the copper substrate, followed by columnar growth to consume the remaining liquid. The columnar austenite grains have lateral dimensions of a few microns, in agreement with previous investigations of rapidly

solidified Fe alloys (5,12,20), and exhibit a slight through-thickness <100> solidification texture, as might be expected for either plane-front or dendritic solidification near the nucleating surface (21).

There is no evidence of microsegregation in TPQ Fe-25%Ni specimens. In MS Fe-Ni ribbons, a segregation-free zone extends from the bottom surface to a position ~1/4 - 1/2 way through the ribbon thickness; in the remainder of each ribbon, the columnar austenite grains contain internal columnar cells associated with slight Ni segregation into the cell boundaries. In several other rapidly solidified alloys, a featureless microstructure adjacent to the substrate has been interpreted as a segregation-free solidification zone (18,22,23). However, the present results are the first direct evidence that the initial stages of rapid solidification in a single-phase alloy can take place without microsegregation, and that this may either continue throughout the solidification process as in TPQ Fe-25%Ni, or may give way to a cellular segregated microstructure as in MS Fe-Ni ribbons. Previously published micrographs of melt-extracted Fe-40%Ni (24) and TPQ Fe-25%Ni (25) also show a segregation-free zone extending ~1/4 - 1/2 way through the specimen thickness, but the authors do not comment on this aspect of the microstructure. In the previous study of TPQ Fe-25%Ni (25), both the measured cooling rate, (6,26) and the extent of the segregation-free zone are smaller than the present results for TPQ Fe-25%Ni, but similar to the present results for MS Fe-Ni ribbons. This suggests that the extent of the segregation-free zone increases with increasing cooling rate, but is not sensitive to differences between TPQ and MS rapid solidification techniques. This is also borne out by the frequent observation of a segregation-free zone in thin areas of gun-quenched alloys (23), which are thought to solidify

at very high cooling rates (14).

Strachan (26) has measured cooling rates of 10^5 - 10^6 K s^{-1} in TPQ Fe-25%Ni, and detected liquid undercoolings of 50-190K before the onset of solidification. The freezing range in Fe-Ni alloys is ∿20K between ∿ 10% and 40%Ni, and at the high undercoolings reported by Strachan, solidification is likely to take place by a massive transformation mechanism, with the solid which is forming having the same bulk alloy composition as the liquid. Massive solidification is thermodynamically feasible when the free energy of the solid is lower than the liquid, i.e. below the T_o temperature, (approximately halfway between the liquidus and solidus temperatures). The solid-liquid interface temperature must fall some way below T_o before massive solidification is favoured kinetically, and the transition point is somewhere between T_o and the solidus temperature (27-30).

Latent heat of solidification is either removed by the cooling substrate or causes recalescence of the solidifying material. For a planar solidification front a distance X from the substrate, conservation of heat under Newtonian conditions gives (15);

$$L\rho\dot{X} = h(T - T_s) + d\rho C\dot{T} \qquad (6)$$

where L is the latent heat of solidification per unit mass, $\dot{X}$ is the instantaneous solid-liquid interface velocity, and $\dot{T}$ is now the instantaneous average rate of increase of specimen temperature. With linear solidification kinetics, $\dot{X} = M(T_L - T)$ where M is the solid-liquid interface mobility and T_L is the liquidus temperature, and the differential equation (6) can be integrated to give (15):

$$X/d = B(\Delta T_N - \Delta T) - AB\Delta T_s \ell n\{(\Delta T - A\Delta T_s)/(\Delta T_N - A\Delta T_s)\} \quad (7)$$

where $A = a/(1 + a)$, $a = h/L\rho M$, $B = b/(1 + a)$, $b = C/L$, $\Delta T = T_L - T$, $\Delta T_s = T_L - T_s$, $\Delta T_N = T_L - T_N$ and T_N is the temperature at the onset of solidification i.e. the nucleation temperature. For pure Fe at high temperature, $\rho = 7.38 \times 10^3$ Kg m^{-3}, $C = 791$ J Kg^{-1} K^{-1} and $L = 2.7 \times 10^5$ JKg^{-1} (31). Taking $h = 10^5 - 10^6$ W m^{-2} K^{-1} and $M = 0.1 - 1.0$ ms^{-1} K^{-1} (32) gives a $\sim 5 \times 10^{-4}$ and b $\sim 3 \times 10^{-3}$ K^{-1}. The last term in eq (7) can then be neglected so that:

$$X/d = b(\Delta T_N - \Delta T) \quad (8)$$

This corresponds to adiabatic recalescence, with no heat removed from the specimen during solidification.

Consider the present results on MS Fe-30, 35 and 40%Ni with a cooling rate at the melting point of 5×10^5 K s^{-1}, together with previous results on TPQ Fe-25%Ni (25) with a cooling rate of $10^5 - 10^6$ K-s^{-1} (6,26) and previous results on melt extracted Fe-40%Ni. In each case, the onset of segregation i.e. ΔT = 10-20K is when X/d = 1/4 - 1/2. Eq (8) indicates that ΔT_N = 93-187K, in good agreement with Strachan's measured undercoolings of 50-190K at a cooling rate of $10^5 - 10^6$ K S^{-1}. The present results show no microsegregation in TPQ Fe-25%Ni and eq (8) indicates that ΔT_N >343K, presumably as a consequence of the higher measured cooling rate at the melting point of $4 \times 10^6 - 10^7$ K s^{-1}. The estimated nucleation undercoolings may be slightly larger when allowance is made for liquid → austenite solidification in Fe-Ni compared with liquid → ferrite solidification in pure Fe. Thus, $C = 595$ J Kg^{-1} K^{-1} and L 3×10^5 J Kg^{-1} at high temperature in austenitic pure Ni, and eq (8) then indicates ΔT_N = 135-270K for the MS conditions of X/d = 1/4 - 1/2 when

ΔT = 10-20K. Allowing for non-Newtonian conditions does not invalidate the use of eq (8), since cooling can only be slower with a given value of h. However, non-Newtonian cooling will concentrate latent heat and therefore recalescence in the region of the solid-liquid interface, building up a temperature inversion ahead of the solid-liquid interface, and leading to thermal rather than constitutional dendritic breakdown of the planar solid-liquid interface. This may explain the convoluted grain shapes found frequently in TPQ Fe-25%Ni.

CONCLUSIONS

Cooling rate measurements indicate non-Newtonian cooling conditions during rapid solidification, with a heat transfer coefficient of 10^5 - 10^6 W m^{-2} K^{-1}. When austenitic Fe-Ni alloys are rapidly solidified, the liquid undercooling before the onset of solidification is more than 300K at a cooling rate of $5x10^6$ - 10^7 K s^{-1}, and 50-200K at a cooling rate of $5x10^5$ K s^{-1}. Solidification then takes place under conditions of adiabatic recalescence. At $5x10^6$ - 10^7 K s^{-1}, the resulting microstructure consists of segregation-free massively-solidified columnar grains, which are a few microns in width and exhibit a slight <100> solidification texture. Convoluted grain boundaries suggest that thermal dendritic breakdown may take place because of recalescence in the later stages of solidification. At $5x10^5$ K s^{-1}, the resulting microstructure consists of an initial region of segregation-free massively-solidified columnar grains, which are again a few microns in width, with a slight <100> texture, but cellular breakdown in the later stages of solidification is caused by Ni microsegregation during recalescence.

ACKNOWLEDGEMENTS

We would like to thank the Science and Engineering Research Council (U.K.) for supporting this research programme. One of the authors (J.J.R.) would also like to acknowledge the partial support of the Director, Office of Energy Research, Office of Basic Energy Sciences, Materials Sciences Division of the U.S. Department of Energy under Contract No. DE-AC03-76SF00098.

REFERENCES

1. N. J. Grant and B. C. Giessen, eds., "Rapidly Quenched Metals II" Vol. 1, MIT Press, Cambridge, Mass, (1976), and Vol. II, Mater Sci. Eng., Vol. 23, (1976).
2. B. Cantor, ed., "Rapidly Quenched Metals III", Metals Society, London, (1978).
3. R. Mehrabian, B. H. Kear and M. Cohen, eds., "Rapid Solidification Processing I", Claitors, Baton Rouge, Louisiana, (1978).
4. R. Mehrabian, B. H. Kear and M. Cohen, eds., "Rapid Solidification Processing II", Claitors, Baton Rouge, Louisiana, (1980).
5. F. Duflos and B. Cantor, Acta Metall. 30, 323 (1982).
6. W. E. Brower, R. W. Strachan and M.C. Flemings, Cast Metal Res. J. 6, 176 (1970).
7. J. V. Wood, P. F. Mills, A. R. Waugh and J. V. Bee, J. Mater. Sci. 15, 2709 (1980).
8. Y. Inokuti and B. Cantor, Acta Metall. 30, 343 (1982).
9. J. J. Rayment and B. Cantor, Metall. Trans. 12A, 1557 (1981).
10. R. W. Cahn, K. D. Krishnanand, M. Laridjani, M. Greenholz and R. Hill, Mater. Sci. Eng. 23, 83 (1976).
11. F. Duflos, D. Phil, Thesis, Sussex, UK (1979).
12. J. V. Wood and R. W. K. Honeycombe in "Ultra Rapid Quenching of Metals", ed. H. Herman, Academic Press, New York, in press.
13. R. C. Ruhl, Mater. Sci. Eng. 1, 313 (1967).
14. H. Jones, Pre. Prog. Phys. 36 1425 (1973).
15. B. Cantor in"Proceedings of the Materials Research Society Symposium on Rapidly Quenched Metals", Boston (1981) in press.

16. W. S. Owen and E. A. Wilson in "Physical Properties of Martensite and Bainite", Iron and Steel Institute, London (1965), p. 53.

17. Y. Inokuti and B. Cantor, Scripta Metall. 10, 655 (1976).

18. J. J. Rayment, O. Ashiru and B. Cantor in "Proc. Int. Conf. on Solid/Solid Phase Transformations", Pittsburgh, PA (1981), in press.

19. C. Hayzelden and B. Cantor, to be published.

20. Y. Inokuti and B. Cantor, J. Mater. Sci. 12, 946 (1977).

21. B. Chalmers, "Principles of Solidification", Wiley, New York, (1964).

22. J. V. Wood and R.W.K. Honeycombe, J. Mater. Sci. 9, 1183 (1974).

23. H. Jones, "Rapid Solidification of Metals and Alloys", Institution of Metallurgists, Monograph No. 8 (1982).

24. S. R. Robertson, T. J. Gorsuch and R.P.I. Adler in reference 3, p. 188.

25. T. Z. Kattamis, W. E. Brower and R. Mehrabian, J. Crystal Growth 19, 229 (1973).

26. R. W. Strachan, Ph.D. Thesis, MIT (1967).

27. M. Hillert in "Lectures on the Theory of Phase Transformations", ed. H. I. Aaronson, AIME, New York (1977).

28. J. C. Baker and J. W. Cahn, Acta Metall. 17, 575 (1969).

29. M. Hillert and B. Sundman, Acta Metall. 25, 11 (1977).

30. S. R. Coriell and R. F. Sekerka in reference 3, p. 35.

31. C. J. Smithells and E. A. Brandes, "Metals Reference Book", Butterworths, London (1976).

32. D. R. H. Jones and G. A. Chadwick, Phil. Mag. 24, 1327 (1971).

Rapid Solidification Technique	Specimen Thickness (μm)	Cooling Rate ($K\ s^{-1}$)			
		1500°C	1000°C	700°C	500°C
TPQ	50	10^7	2×10^6	9×10^5	3×10^5
TPQ	100	4×10^6	7×10^5	10^5	4×10^4
MS	40	5×10^5	10^4	-	-

Table 1: Measured cooling rates during rapid solidification

Rapid Solidification Technique	Nominal Composition (wt%Ni)	Measured Composition (wt%Ni)	Vickers Microhardness (Kg mm^{-2})
TPQ	25	25.0	270
MS	30	29.4	170
MS	35	34.3	150
MS	40	39.3	175

Table 2: Wave dispersive spectroscopic analysis of compositions and microhardness values in rapidly solidified Fe-Ni alloys.

Rapid Solidification Technique	Austenite Grain Size (μm)	Cell size (μm)	Dislocation Density ($lines\ m^{-2}$)
TPQ	1.0-3.0	-	10^{15}
MS (bottom surface)	1.5-2.5	-	10^{12}
MS (top surface)	2.0-6.0	0.5-1.5	10^{12}

Table 3: Austenite grain size, cell size, and dislocation density in rapidly solidified Fe-Ni alloys.

Nominal Alloy Composition (wt%Ni)	Take off Angle	EDS Analysis of Cell Centres and Boundaries			
		Number of Data Points	Cell Centres (wt%Ni)	Number of Data Points	Cell Boundaries (wt%Ni)
30	38	10	28.7±1.5	8	28.9±1.9
30	25	17	27.0±0.6	18	28.1±0.9
35	20	15	32.9±0.9	21	33.3±1.3
35	25	6	32.2±1.2	10	32.7±1.3
35	25	7	32.2±0.9	10	32.5±0.8
40	25	12	38.6±2.3	15	40.6±1.8

Table 4: Energy Dispersive Spectroscopic analysis of compositions at cell centres and cell boundaries in cellular austenitic specimens from different melt-spun Fe-Ni ribbon specimens.

FIGURE CAPTIONS

Fig. 1. Transverse microstructure of columnar austenite grains in two piston quenched Fe-25%Ni.

Fig. 2. Transverse microstructure of columnar austenite grains with convoluted grain boundaries in two piston quenched Fe-25%Ni.

Fig. 3. Transverse microstructure of columnar austenite grains near the bottom surface of melt-spun Fe-35%Ni.

Fig. 4. Transverse microstructure of columnar austenite grains near the top surface of melt-spun Fe-35%Ni, showing a cellular segregation structure within the austenite grains.

Fig. 5. Through-thickness of melt-spun Fe-30%Ni. The solidification direction is upwards, the black heavily-etched lines are columnar austenite grain boundaries, and the light lines in the upper half of the micrograph show columnar cells within the austenite grains.

Fig. 6. The same region as in Figure 4 after tilting slightly to image dislocations in the right-hand grain decorating the cell boundaries.

Fig. 7. (a) Two-piston quenched Fe-25%Ni;

(b) Relative orientations of unit stereographic triangles obtained by Kikuchi line analysis from each of the 8 austenite grains in (a).

Fig. 8. (a) Melt-spun Fe-35%Ni;

(b) Relative orientations of unit stereographic triangles obtained by Kikuchi line analysis from each of the 5 austenite grains in (a).

Fig. 9. Calculated variation of mean cooling rates ($\dot{T}$) versus specimen thickness (d) for different values of heat transfer coefficient (h), together with experimental data for Al and Fe alloys. Open triangles and squares are the present data for two-piston quenched and melt-spun Fe-Ni alloys respectively; open circles are previous data for rapidly solidified Fe-Ni from references 6, 25 and 26; filled circles are previous data for rapidly solidified Al alloys from reference 14.

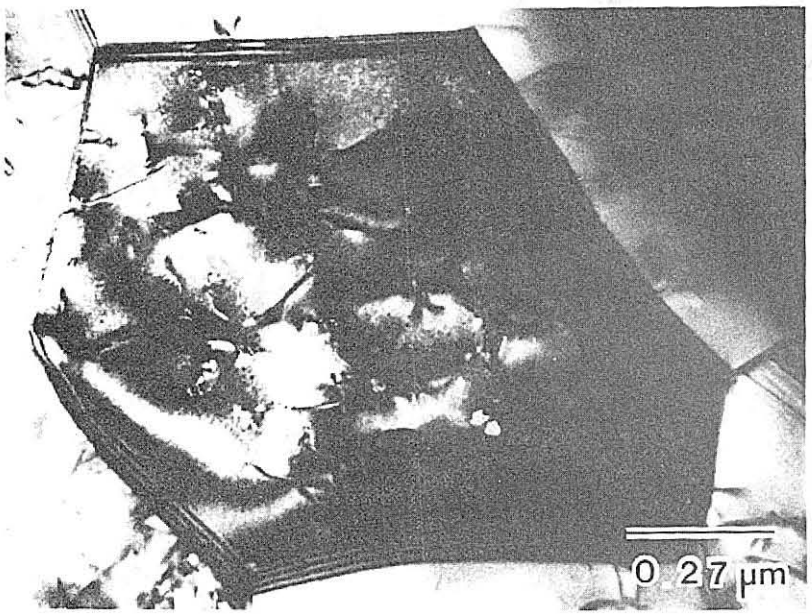

Figure 1

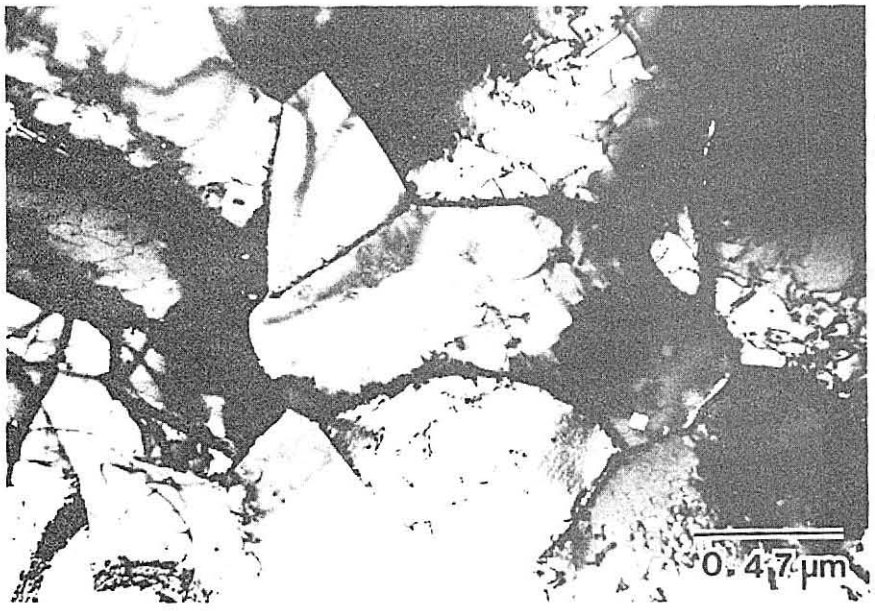

XBB 827-6598

Figure 2

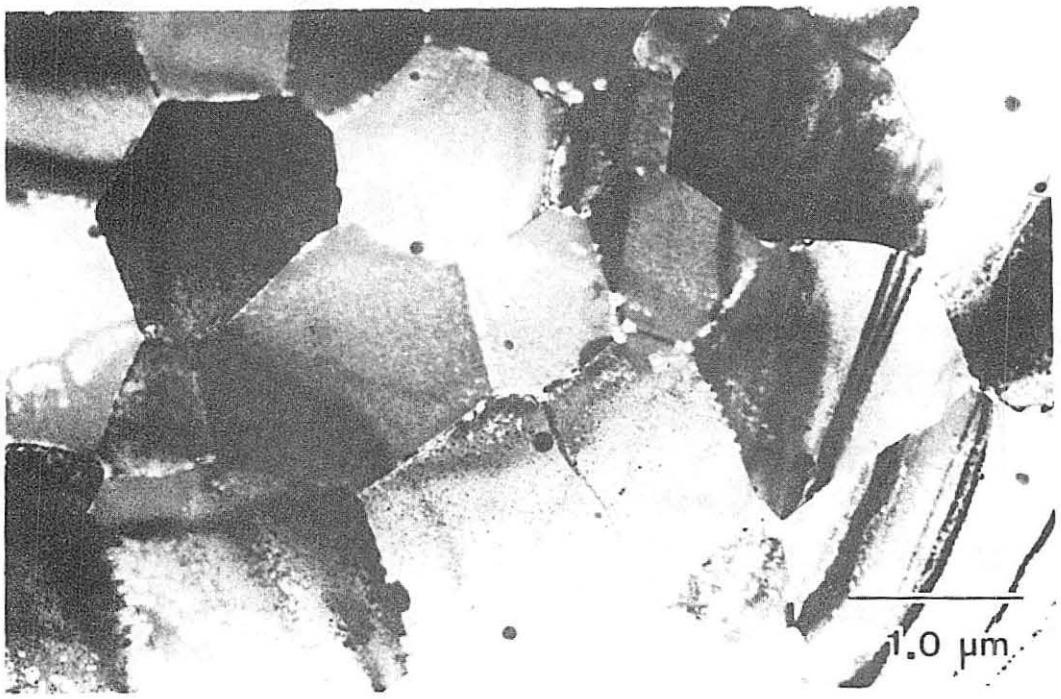

Figure 3

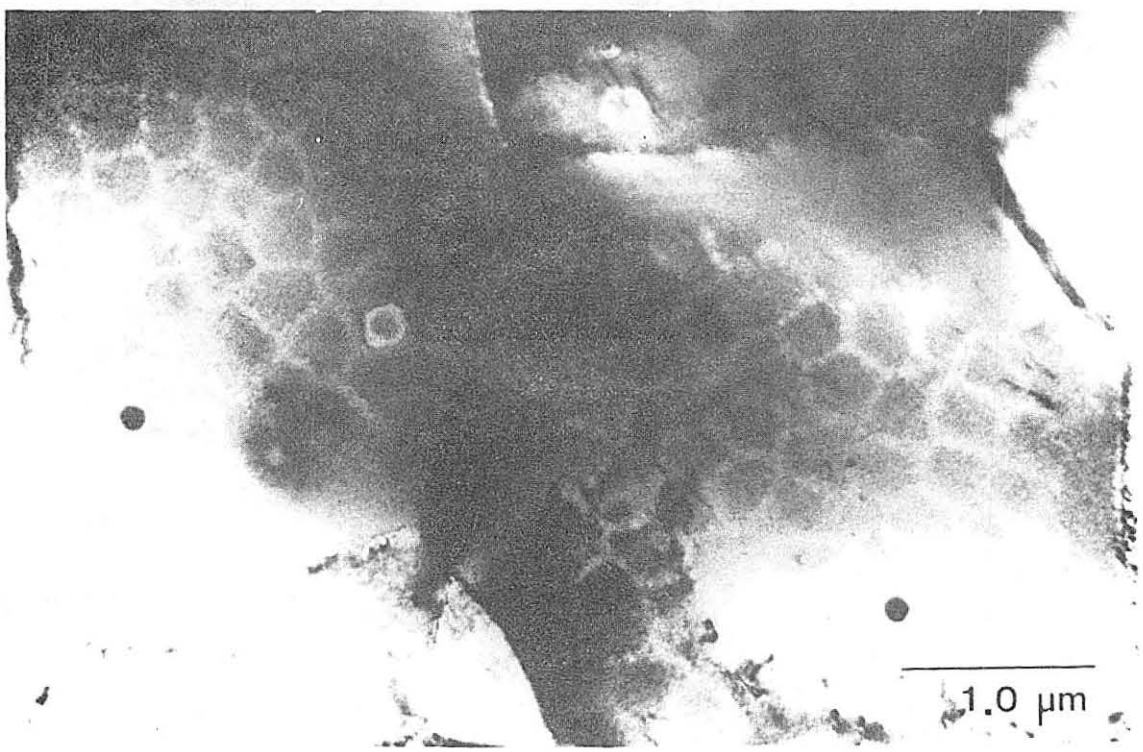

XBB 827-6599

Figure 4

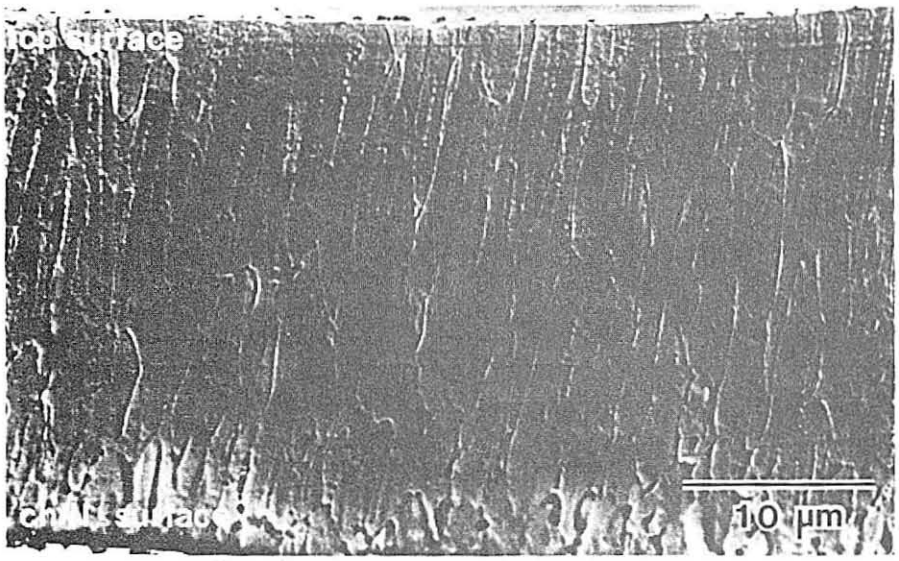

Figure 5

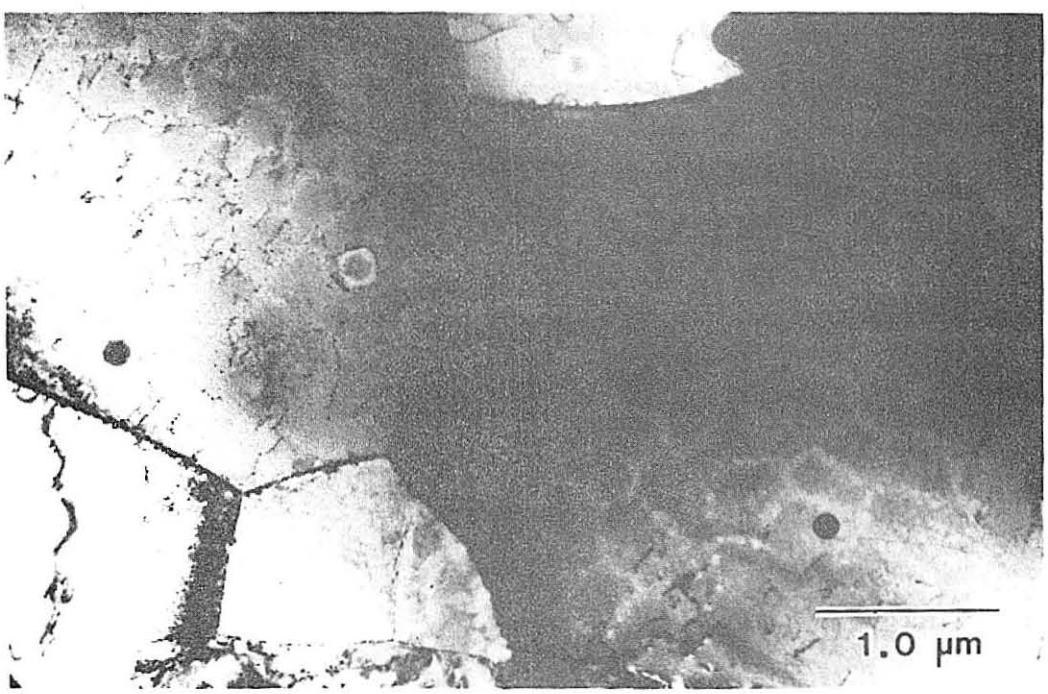

XBB 827-6600

Figure 6

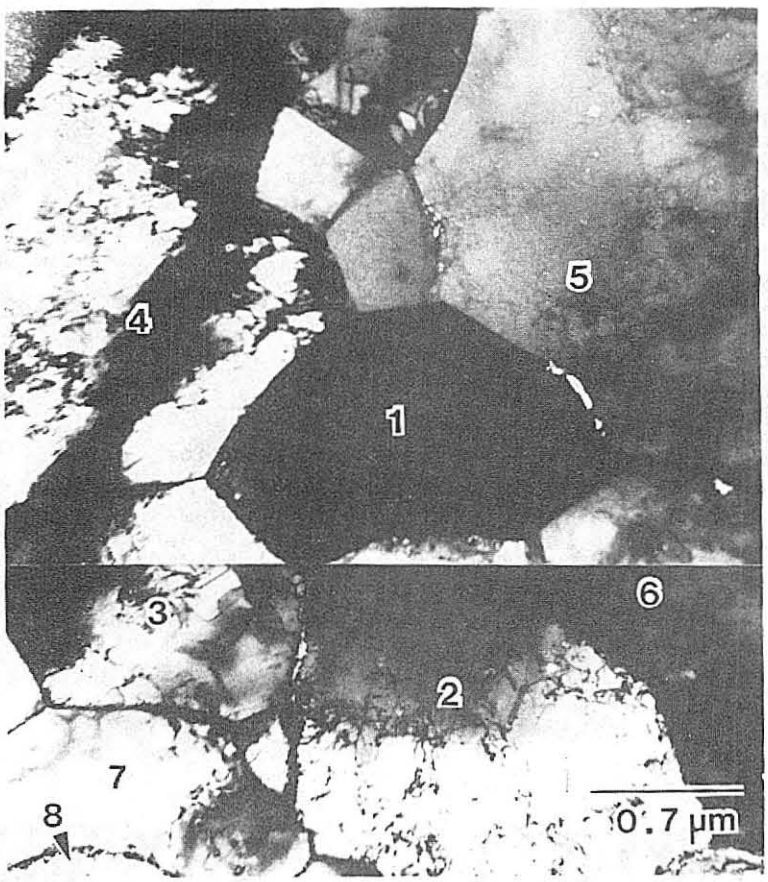

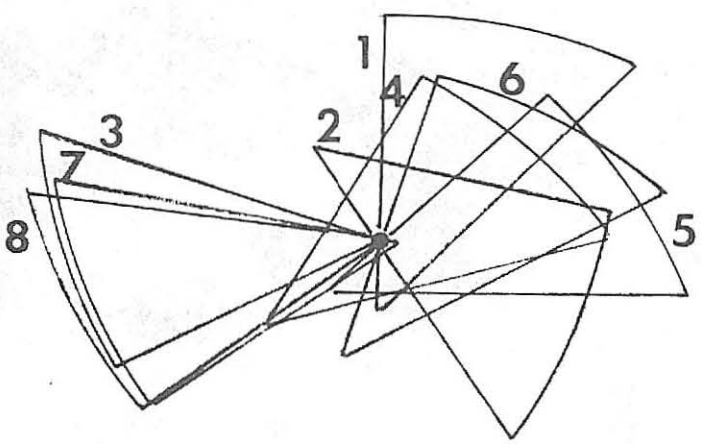

XBB 827-6596

Figure 7a-b

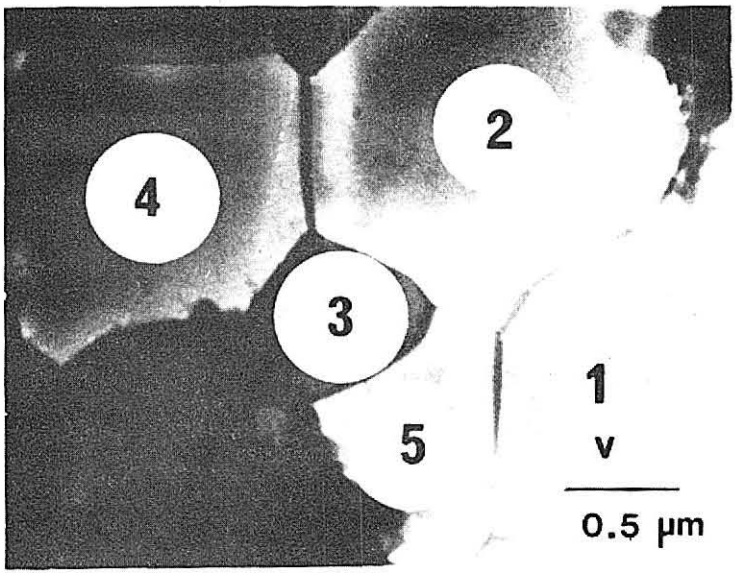

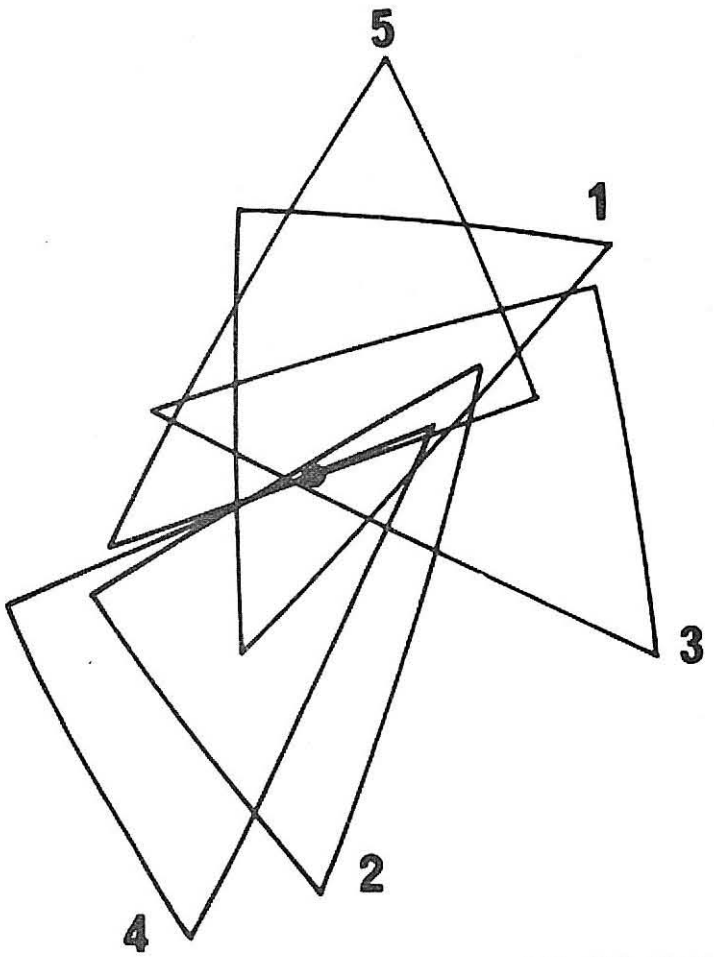

XBB 827-6597

Figure 8a-b

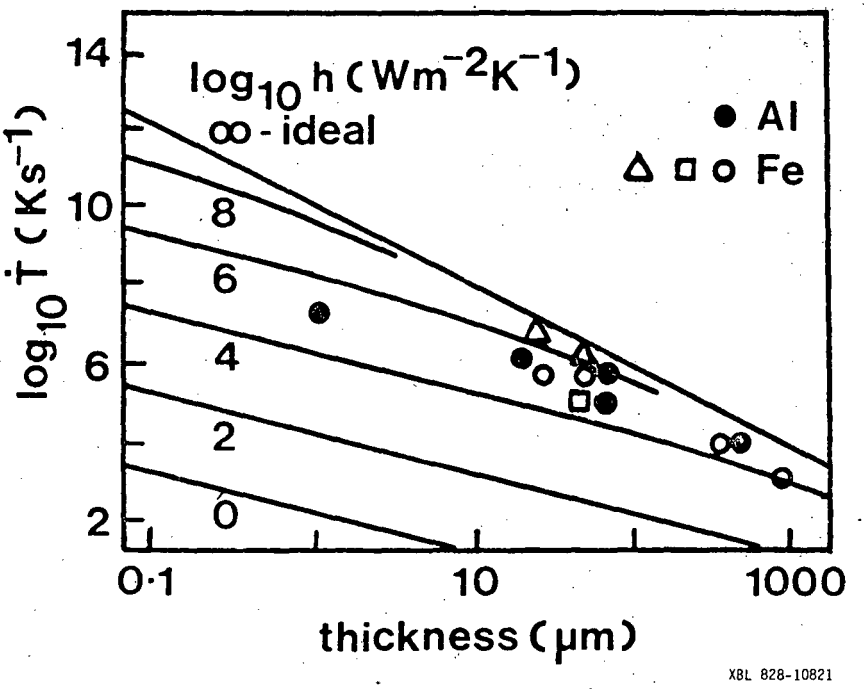
14
10
6
2
$\log_{10} \dot{T}$ (Ks^{-1})
$\log_{10} h$ ($Wm^{-2}K^{-1}$)
∞ - ideal
8
6
4
2
0
● Al
Δ □ ○ Fe
0·1
10
1000
thickness (μm)
XBL 828-10821

Figure 9

TECHNICAL INFORMATION DEPARTMENT
LAWRENCE BERKELEY LABORATORY
UNIVERSITY OF CALIFORNIA
BERKELEY, CALIFORNIA 94720